

RESEARCH PAPER

Synthesis of Magnesium Ferrite-Silver Nanostructures and Investigation of its Photo-catalyst and Magnetic Properties

Sadaf Samiei , Fatemeh Pakpour*, Davood Ghanbari

Department of Science, Arak University of Technology, Arak, Iran

ARTICLE INFO

Article History:

Received 11 October 2017

Accepted 17 December 2017

Published 01 January 2018

Keywords:

Magnesium Ferrite

Magnetic; Nanostructure

Nanocomposite

Photo-catalyst

ABSTRACT

In this research we first synthesized $MgFe_2O_4$ nanostructures via hydrothermal method using $(Mg(NO_3)_2 \cdot 6H_2O)$ and $(Fe(NO_3)_3 \cdot 9H_2O)$. The influence of concentration, surfactant, precipitating agent and temperature on the particle size and magnetic properties of the synthesised nanoparticles were examined. Then $MgFe_2O_4$ -Ag nanocomposites were prepared by a simple chemical precipitation. The structural characteristics of samples were studied by X-ray diffraction (XRD), scanning electron microscopy (SEM), and Fourier transform infrared (FT-IR). Spectroscopy vibrating sample magnetometer showed that the prepared ferrite nanostructures had ferromagnetic property. The photocatalytic aspects of $MgFe_2O_4$ -Ag nanoparticles and nanocomposites were measured using the degradation of three azo dyes (acid red, acid violet and methyl orange) under ultraviolet irradiation. Our results confirm the successful formation of $MgFe_2O_4$ nanoparticles and $MgFe_2O_4$ -Ag nanocomposite. It was also shown that the prepared nanostructures had appropriate magnetic properties and photocatalytic performance.

How to cite this article

Samiei S, Pakpour F, Ghanbari D. Synthesis of Magnesium Ferrite-Silver Nanostructures and Investigation of Its Photo-catalyst and Magnetic Properties. J Nanostruct, 2018; 8(1): 37-46. DOI: 10.22052/JNS.2018.01.005

INTRODUCTION

Magnesium ferrite with a cubic spinel structure has unique magnetic properties. Because of the special electronic structure it shows peculiar magnetic properties as the particles reach a certain size [1]. It has also peculiar properties such as low melting point, large expansion coefficient, high specific heat and low magnetic transition temperature [2,3] which make it suitable for many applications such as ferro-fluid technology, information storage, transformers and cores of coils [4,5], gas sensors [6], catalysts [7], brown pigments [8], and so on. Over the past two decades, photocatalytic decomposition processes have also shown high potential for coloured and contaminated wastewater purification [9].

Ferrite compounds with general formula of XFe_2O_4 , where X can be Co, Ni, Mg, etc., have a

* Corresponding Author Email: fpakpour@gmail.com

cubic close pack structure [10]. $MgFe_2O_4$ is also a soft magnetic n-type semiconductor with a band gap of 2.18 eV [11]. It is also known that one of the most important photocatalysts are metal oxide nanoparticles [12]. Nanoparticles of magnesium ferrite, even in large sizes, have paramagnetic cloud characteristics, because magnetic inhomogeneity in magnesium ferrite can be less than other spinel ferrites in which all of the cations have a larger magnetic momentum [13, 14]. In terms of $MgFe_2O_4$ nanocomposites, the type of the semiconductor additive to the magnetic core will be of particular importance in the final properties of the nanocomposite.

Among the AOP (Advanced Oxidation Processes), one of the most economical methods is the use of photocatalyst under light irradiation. This process uses ultraviolet light to stimulate a



This work is licensed under the Creative Commons Attribution 4.0 International License.

To view a copy of this license, visit <http://creativecommons.org/licenses/by/4.0/>.

semiconducting material as a photocatalyst and cause complete destruction of pollutants into harmless compounds.

Then using semiconductor based photocatalysis could overcome to the disadvantages of the traditional water purification's methods. This applicable and green method can degrade various harmful organic compounds to smaller fragments and finally to H_2O/CO_2 as hydroxyl and superoxide radicals attacking organic matters [15,16]. During irradiating a semiconducting material by ultraviolet or visible photons with sufficient energy, photo generated electron-hole pairs react with dissolved oxygen and water/hydroxyl ions to form superoxide and hydroxyl radicals, respectively. One of the main problems of heterogeneous photocatalysis is recombination of electron-hole pairs which significantly decreases the photocatalytic efficiency [17-21].

MATERIALS AND METHODS

$Mg(NO_3)_2 \cdot 6H_2O$, $(Fe(NO_3)_3 \cdot 9H_2O)$, NaOH, starch, glucose, citric acid were purchased from Merck company. In this work a simple coprecipitation and hydrothermal methods were applied to produce nanostructures using water as solvent and natural materials as surfactants. We tried not to use harmful chemical solvents. The structural characterization of the nanoparticles was studied using XRD analysis. X-ray diffraction analysis (XRD) applied with $CuK\alpha$ radiation with $\lambda = 1.5418 \text{ \AA}$ in $2\theta = 10-80$ degrees. To evaluate the morphology and size of the particles a scanning electron microscopy was run by the use of a LEO instrument model 1455VP. The surface of the sample were coated by a very thin layer of a conductor (here Pt, using a BAL-TEC SCD 005 sputter coater) to eliminate charge accumulation and to have a clear contrast. A vibrating sample magnetometer (VSM) device, made by Meghnatis Kavir Kashan Company (Iran) was used to study room temperature magnetic properties in an applied magnetic field changing from -10000 Oe to $+10000$ Oe.

Synthesis of $MgFe_2O_4$ nanoparticles

0.5 g of $Mg(NO_3)_2 \cdot 6H_2O$ and 1.57 g of $(Fe(NO_3)_3 \cdot 9H_2O)$ were separately dissolved in 100 ml of distilled water and then mixed. 36 ml of NaOH solution (0.5 molar) was added to this solution until a pH of 8 is reached. The solution was stirred for 15 min, and was maintained at 180 C for 5-24

h at Teflon-autoclave. The formed sediment was washed with distilled water and centrifuged to separate the sediment. The product was dried in a hot air oven at a temperature of 75 °C. The final product was calcined at 500°C and its colour goes from brown to black.

Synthesis of $MgFe_2O_4$ -Ag nanocomposite by hydrothermal

0.1 g of $MgFe_2O_4$ was dispersed in 200 ml of deionised water by mechanical stirrer. Then 0.25 g of $AgNO_3$ was added to the solution. After 60 minutes, when the solution turns black, 30 ml of $NaBH_4$ solution (0.3g) was added to it, then it was placed in an autoclave under 170 ° C, 50 psi pressure and 5 hours. Finally the obtained precipitate was calcined at 850°C.

Photo-catalytic degradation process

5 ml of the dye solution was used as a pollutant model to determine the photocatalytic activity. 0.1 g of catalyst was applied for degradation of 5 ml solution. The solution was irradiated by three 8 W (UV) lamp which was placed in a quartz pipe in the middle of reactor. It was stirring the solution and sampling (about 5 ml) was done every 60 min. The samples were filtered, centrifuged and their concentration was determined by UV-Visible spectrometry.

RESULTS AND DISCUSSION

XRD pattern of synthesised $MgFe_2O_4$ nanoparticles has been illustrated in Fig. 1. As it is seen the XRD pattern reveals the typical diffraction pattern of pure cubic phase (JCPDS No.: 88-1937) with Fd-3m space group which is consistent with pure magnesium ferrite. The composition of the $MgFe_2O_4$ -Ag nanocomposite was also investigated. Presence of both ferrite phase and silver phase were confirmed and illustrated in Fig. 2.

To calculate the crystalline size for $MgFe_2O_4$ Scherrer equation, $D_c = K\lambda/\beta \cos\theta$, was used, where β is FWHM (width of the observed diffraction peak at its half maximum intensity), K is the shape factor, with a value of about 0.9, and λ is the X-ray wavelength ($CuK\alpha$ radiation, equals to 0.154 nm) [22]. The average crystalline size for $MgFe_2O_4$ and $MgFe_2O_4$ -Ag nanoparticles were found to be around 13.8 nm and 20 nm respectively.

The morphology and particle size of the products were estimated by SEM. Fig. 3 shows pure $MgFe_2O_4$ nanoparticles prepared by

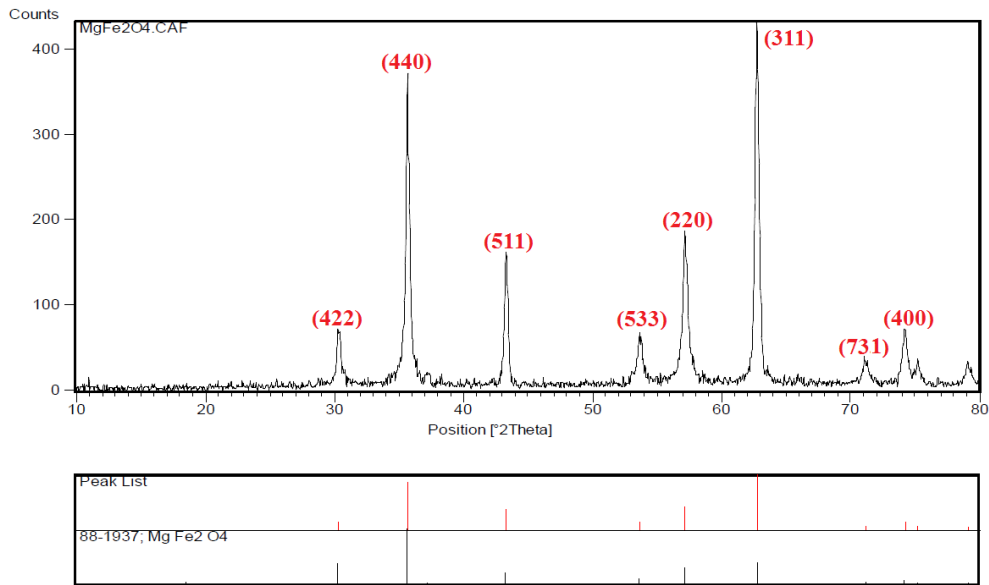


Fig. 1. XRD pattern of MgFe₂O₄ nanoparticles

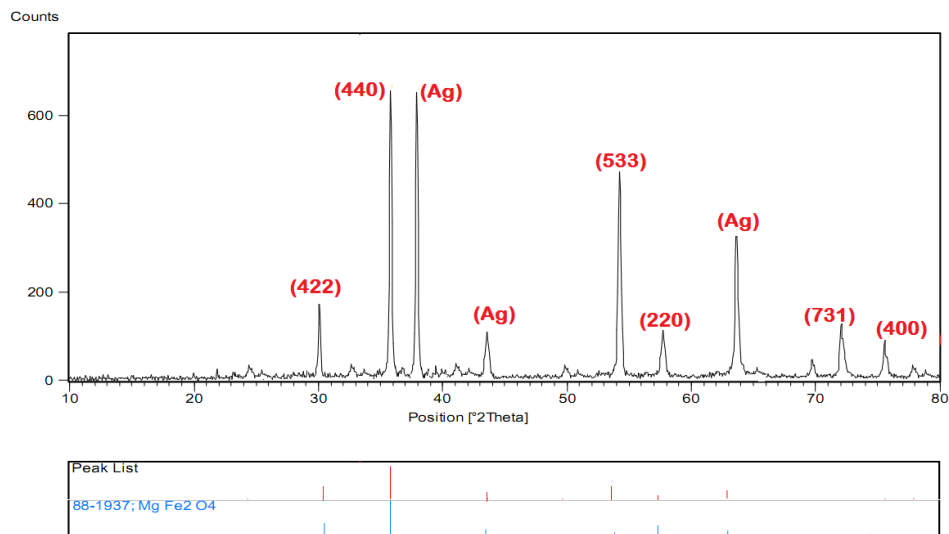


Fig. 2. XRD pattern of MgFe₂O₄-Ag nanocomposite

hydrothermal method. According to scanning electron microscopy images the average particle size is found to be around 50 nm. The particle size and magnetic properties can be easily controlled by changing in precursors. The balance between nucleation and growth rates, determines final particle size so the morphology depends on the preparation conditions. Fig. 4 shows SEM images of MgFe₂O₄ nanoparticles synthesized in 160 ° C for 24 hours. The average particle size is calculated to be around 50 nm. Regarding the shape, we see that the particles are hunch and sticking together.

Fig. 5 shows SEM images of MgFe₂O₄ nanoparticles synthesized in the presence of starch surfactant. The average particle size is calculated to be around 80 nm. According to the pictures, the particles are spherical and regular. SEM image of magnesium ferrite prepared by citric acid coating is shown in Fig. 6. The results show the spherical particles sticking together with a diameter of less than 50 nm. Fig. 7 illustrates SEM images of the MgFe₂O₄ nanoparticles synthesized in the presence of glucose surfactant. As it is seen the particles have regular spherical shape and they are formed at

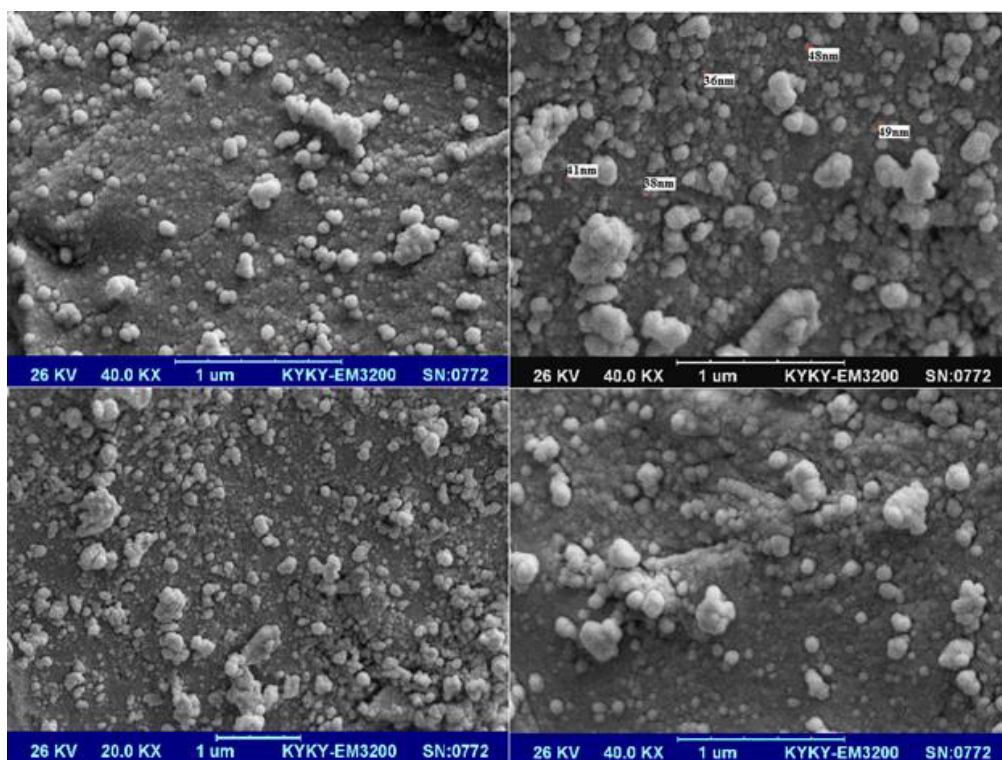


Fig. 3. SEM images of pure magnesium ferrite nanoparticles

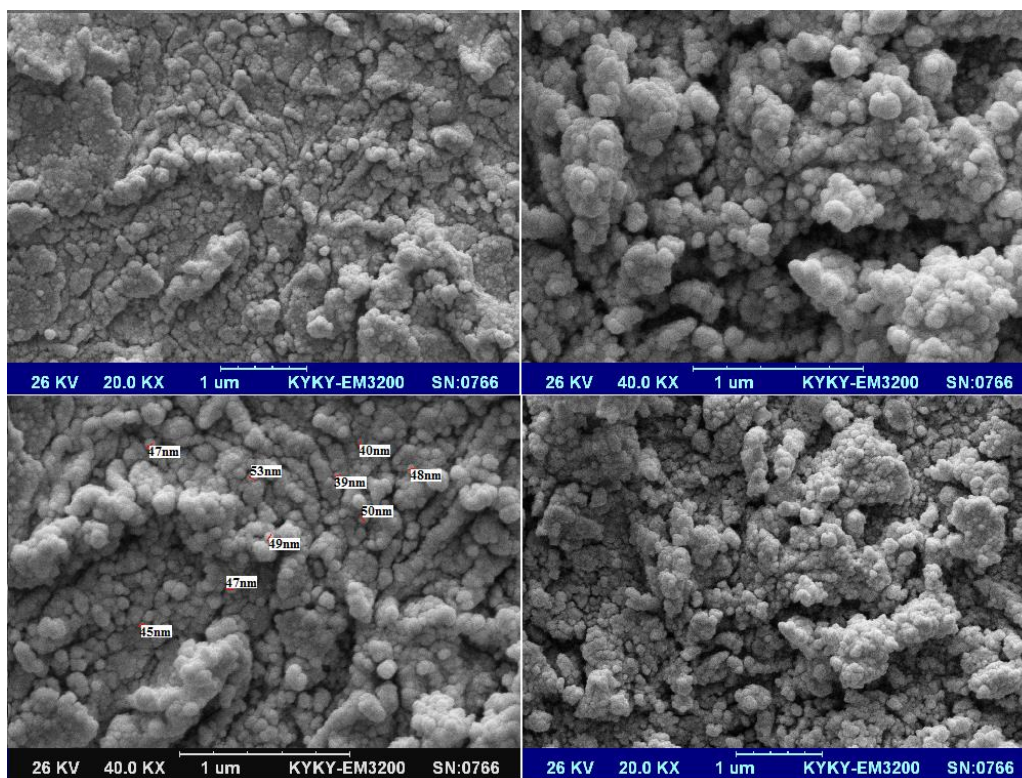


Fig. 4. SEM images of $MgFe_2O_4$ nanoparticles at 24 hours

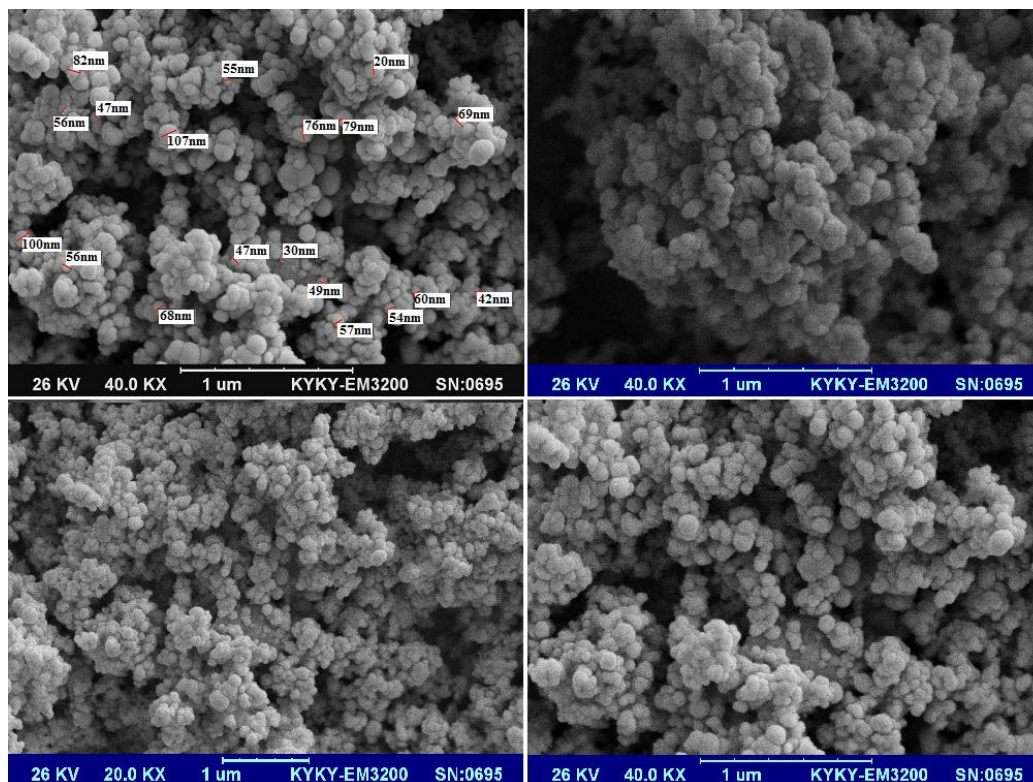


Fig. 5. SEM images of $MgFe_2O_4$ nanoparticles with starch

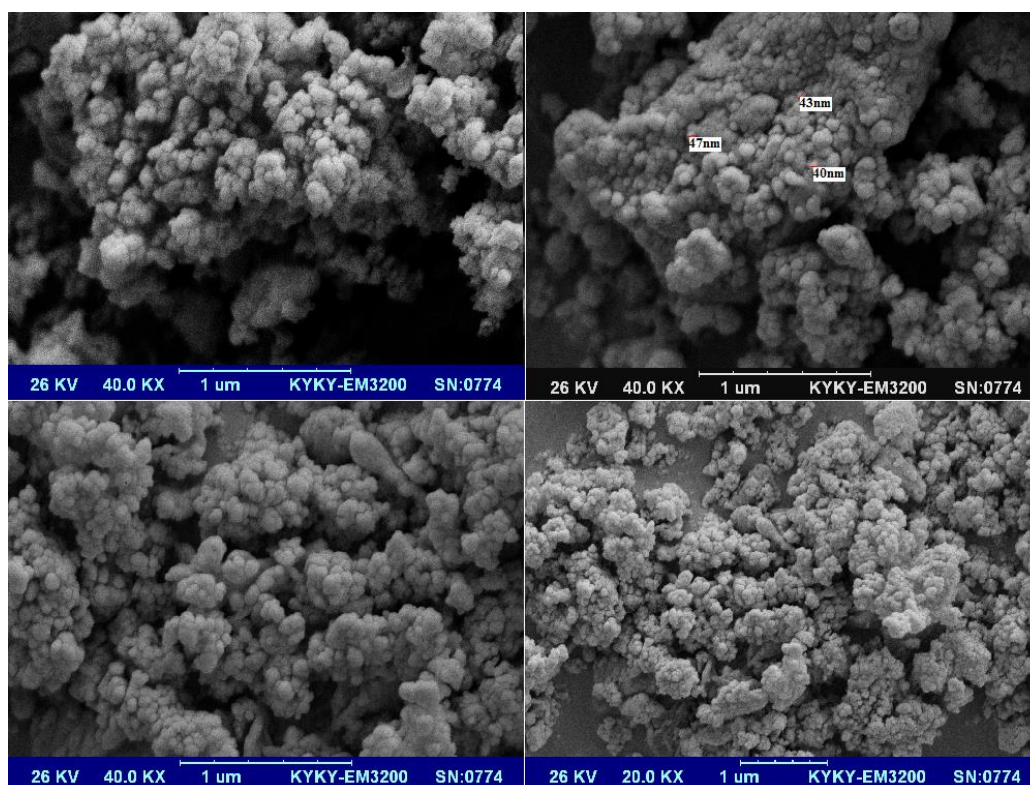


Fig. 6. SEM images of $MgFe_2O_4$ nanoparticles with citric acid

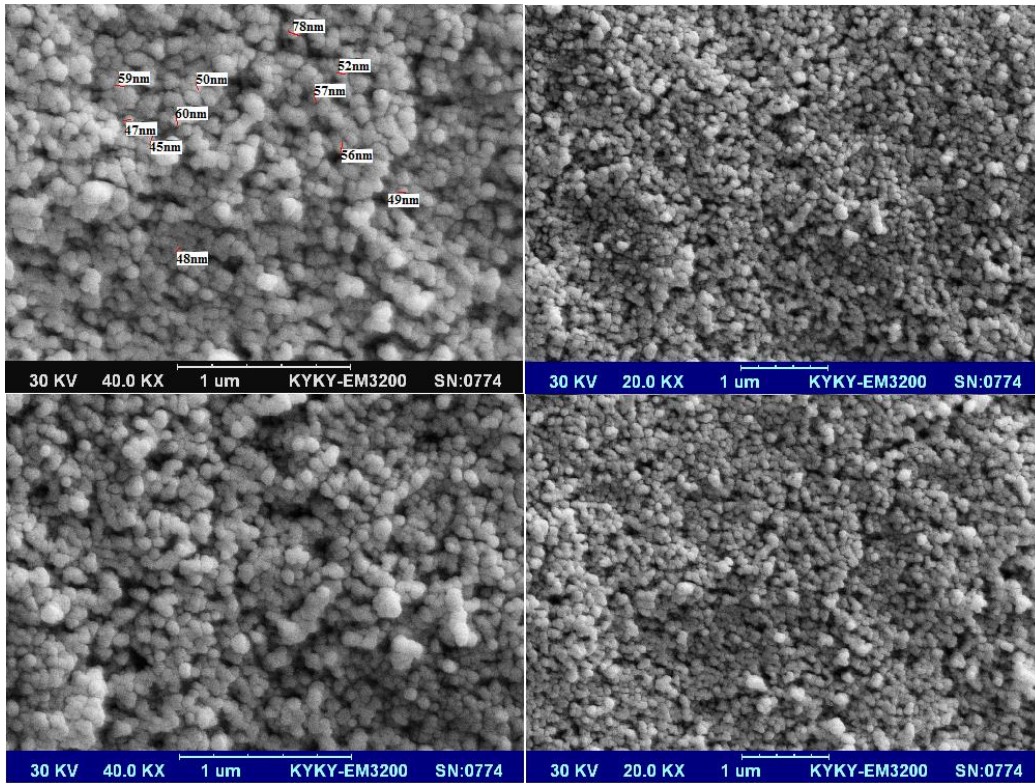


Fig. 7. SEM images of images of the $MgFe_2O_4$ nanoparticles with glucose

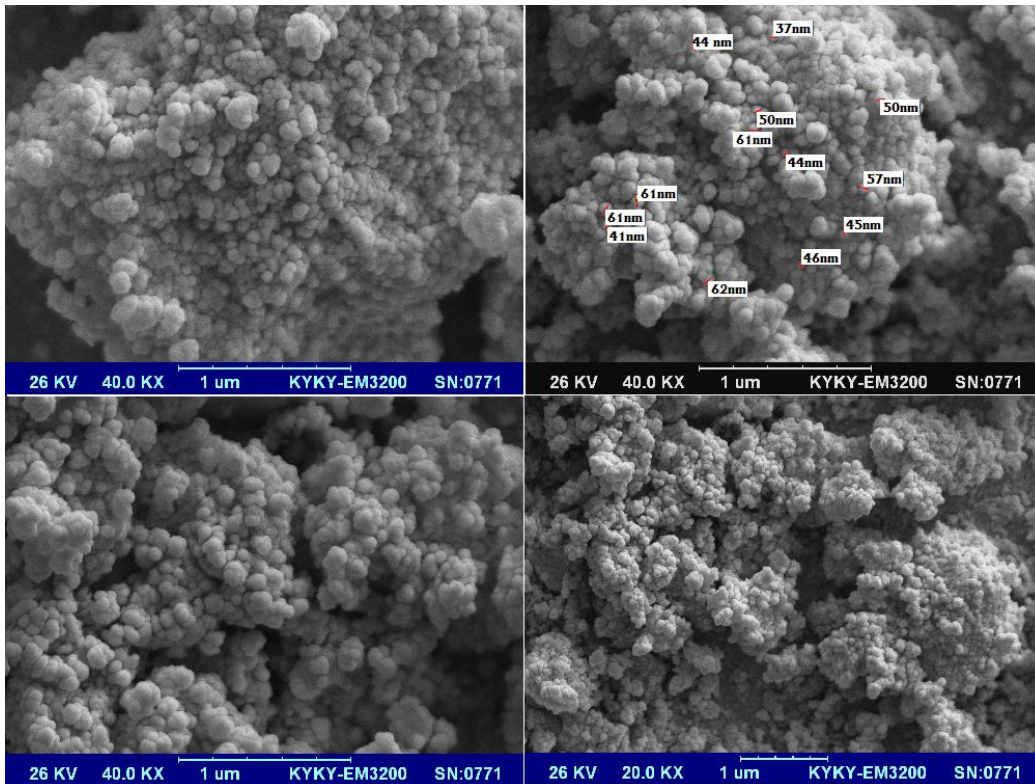


Fig. 8. SEM images of $MgFe_2O_4$ -Ag nanocomposite.

close distances and adhering to each other with an average diameter of less than 80 nm.

Fig.8 illustrates SEM images of synthesized $MgFe_2O_4$ -Ag using hydrothermal method. The resulting image is arranged in the form of spherical particles that are sticking together and irregular and with a diameter of less than 100 nm.

FT-IR spectrum of the synthesized and heat-treated at 160 °C $MgFe_2O_4$ sample obtained by hydrothermal method is shown in Fig. 9a. The spectrum shows prominent band near 3418 cm^{-1} , which are attributed to the stretching modes and O-H vibrations of the free or adsorbed water. The weak band near 1630 cm^{-1} is assigned to H–O–H bending vibration mode due to the adsorption of moisture. Peak corresponding to Metal–Oxygen stretching was observed at 594 cm^{-1} , which is assigned to Fe–O. It suggests that there is a conversion into pure ferrite phase with heat treatment. Fig.9b shows the FT-IR spectrum of the $MgFe_2O_4$ nanoparticles that obtained by citric acid. The band at 603-687 cm^{-1} was assigned to

Mg–O stretching vibration mode. The broad band at 3395 cm^{-1} was assigned to the O–H stretching vibration and the weak band near 1356-1788 cm^{-1} was assigned to H–O–H bending vibration mode. IR spectrum of the as synthesized $MgFe_2O_4$ nanoparticles that obtained by glucose is shown in Fig. 9c. The spectrum shows bands near 3422 cm^{-1} , which are attributed to the stretching modes and O-H bending vibrations of the free or adsorbed water, also the weak band at 1629 cm^{-1} was assigned to H–O–H bending vibration. And peaks corresponding to Metal–Oxygen stretching were observed at 446 and 630 cm^{-1} , which are assigned to Fe–O and Mg–O stretching vibration mode.

Magnetic property of surfactant-free $MgFe_2O_4$ was studied at temperature 160°C using vibration sample magnetometer instrument and is depicted in Fig.10a. The result indicates that, the sample exhibit ferromagnetic property. A saturation magnetization around 2.6 emu/g, and coercivity about 7 Oe have been achieved. Fig.10b shows magnetic property of $MgFe_2O_4$ nanoparticles

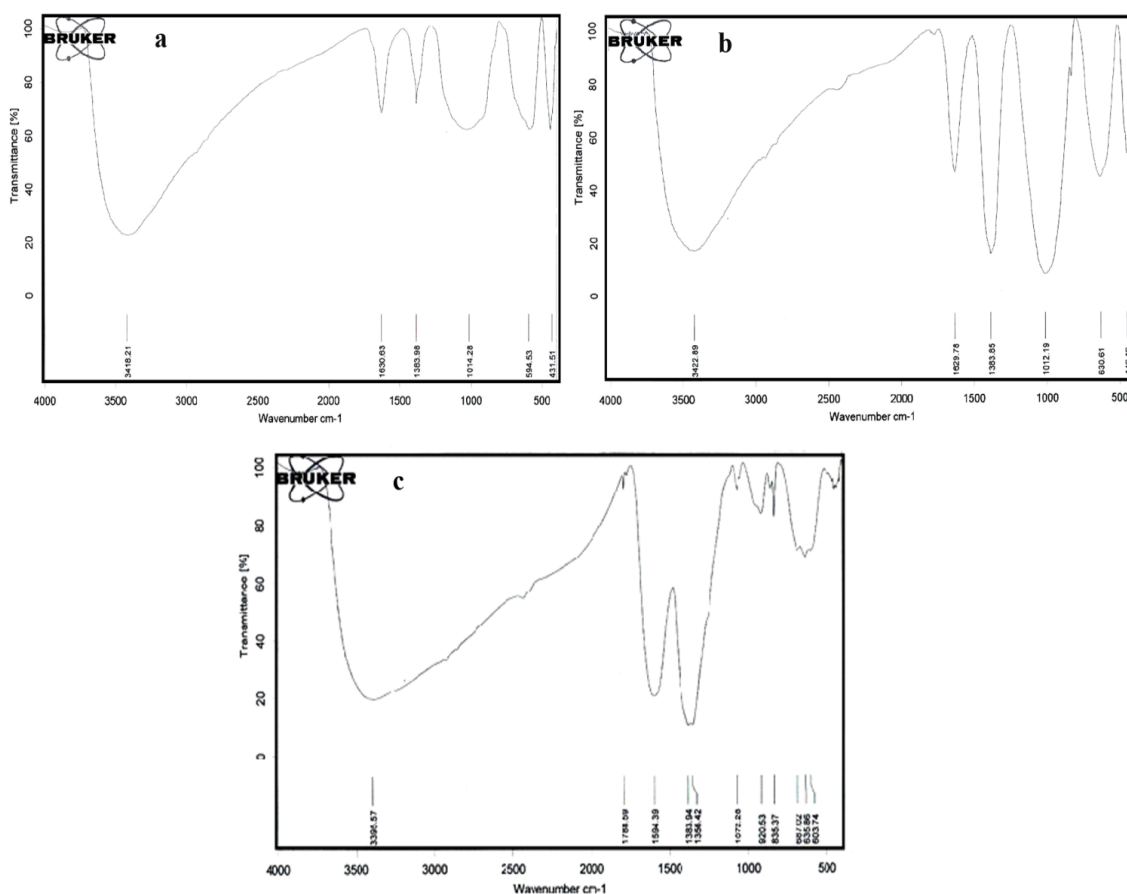


Fig. 9. FT-IR spectrum of a) $MgFe_2O_4$ nanoparticles b) $MgFe_2O_4$ nanoparticles with citric acid c) $MgFe_2O_4$ nanoparticles with glucose

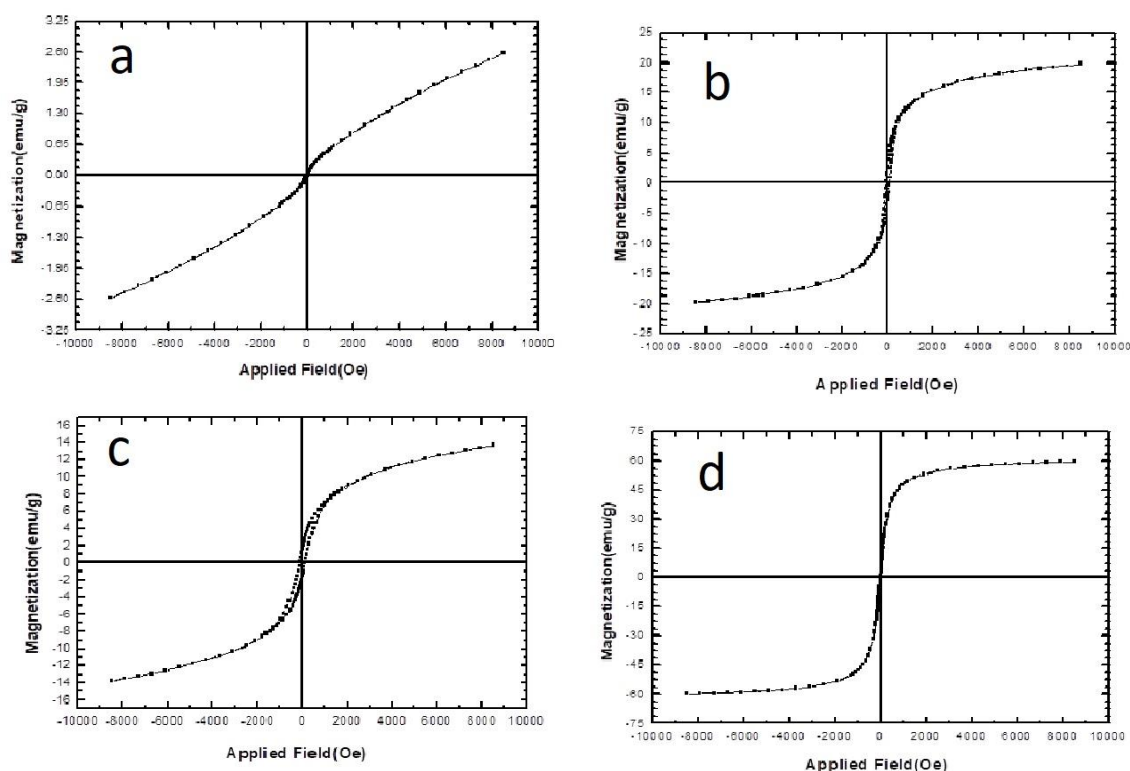


Fig 10. VSM curve of a) MgFe_2O_4 pure nanoparticles at temperature 160°C b) MgFe_2O_4 nanoparticles are calcined at temperature 500°C c) MgFe_2O_4 nanoparticles are calcined at temperature 850°C d) $\text{MgFe}_2\text{O}_4\text{-Ag}$ nanocomposite are calcined at temperature 500°C

that obtained by precipitation and calcinated temperature in 500°C . A saturation magnetization around 20 emu/g , and coercivity about 69 Oe have been achieved. Fig.10c shows magnetic property MgFe_2O_4 nanoparticles that obtained by co-precipitation and calcinated temperature in 850°C . A saturation magnetization around 14 emu/g , and coercivity about 123 Oe have been achieved. Magnetic property of $\text{MgFe}_2\text{O}_4\text{-Ag}$ nanocomposite that obtained and calcinated at temperature equals to 500°C is shown in Fig.10d. A saturation magnetization around 60 emu/g , and coercivity about 6.5 Oe have been achieved. The magnetic property of the prepared nanocomposites is an essential characteristic of a heterogeneous nanocomposite since materials with this magnetic behaviour have low tendency in inter-particles agglomeration caused by dipole-dipole interaction in comparison with ferromagnetic nanocomposites. The results also indicate that nanocomposite formation give rise to coercivity enhancement. The magnetic properties of nanocomposites were affected by

the magnetic exchange interactions between the different phase components.

Acid red, methyl orange and acid violet as typical organic pollutants were employed as targets because of the relative stability of their molecular structure. The as-prepared nanoparticles have the potential to be applied to improve environmental problems associated with organic and toxic water pollutants. Maximum absorption peaks (λ_{max}) of organic dyes that were used for degradation under UV light are obtained from UV-vis absorption spectra and were confirmed by scientific literature. The photo-catalytic activity of the nanoparticles was evaluated by monitoring the degradation of organic dyes in an aqueous solution, under UV irradiation. The changes in the concentration of dye are illustrated in Fig. 11, 12. As time increase; more and more dyes are adsorbed on the nanoparticles catalyst, until the absorption peaks (λ_{max}) of acid red, methyl orange and acid violet decrease and vanish around 120 minutes. The dyes concentration decreased with increasing

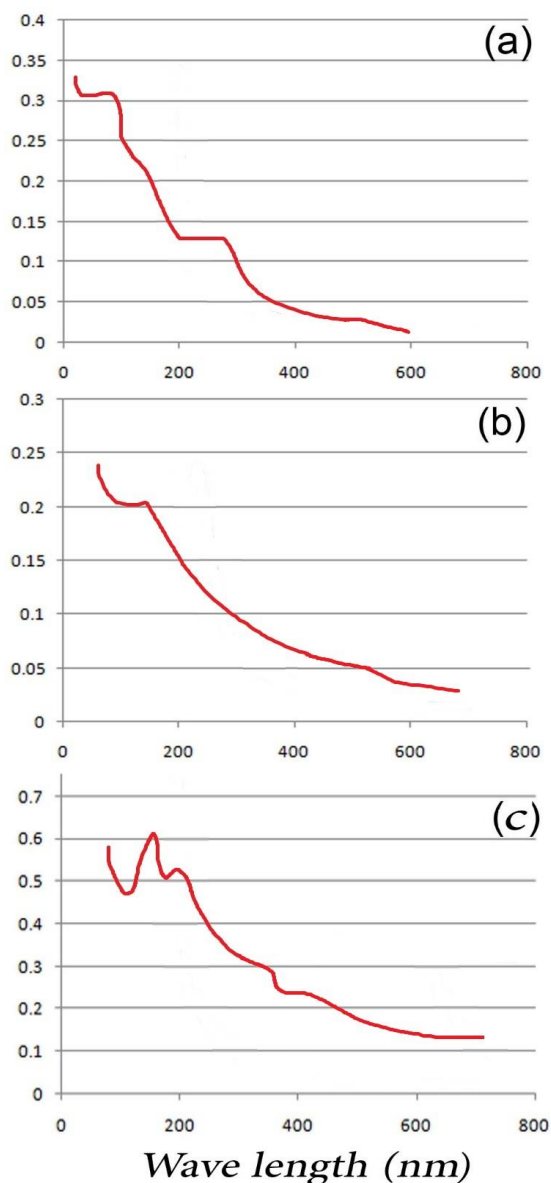


Fig. 11. UV-vis absorption spectra of Mg-ferrite photocatalysts (a) acid red (b) acid violet (c) methyl orange

UV-irradiation time organic dyes decompose to carbon dioxide, water and other less toxic or nontoxic residuals.

CONCLUSIONS

MgFe₂O₄ nanoparticles and MgFe₂O₄-Ag nanocomposite were successfully synthesized using co-precipitation and hydrothermal methods. XRD pattern with well-defined peaks showed the formation of pure magnesium ferrite space group of Fd3m. The ferromagnetic property of synthesised nanostructures was approved by vibrating sample

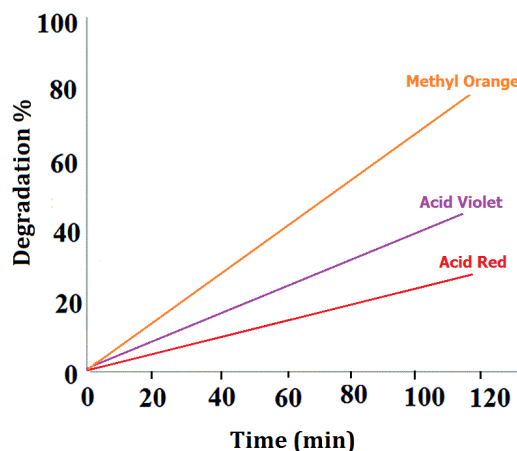


Fig. 12. Decomposition of azo dyes under UV irradiation

magnetometer analysis. It was shown that as the calcination temperature increased the coercivity also increased. The photo-catalytic activity of the nanoparticles was examined by monitoring the degradation of organic dyes in an aqueous solution, under UV irradiation and it was shown that the magnesium ferrite can be promisingly used for photocatalytic purposes.

CONFLICT OF INTEREST

The authors declare that there are no conflicts of interest regarding the publication of this manuscript.

REFERENCES

- Chen Q, Zhang Z.J. Size-dependent superparamagnetic properties of MgFe₂O₄ spinel ferrite nanocrystallites, *Appl. Phys. Lett.*, 1998; 73:3156-3158.
- Xu Q., Wei Y., Liu Y., Ji X., Yang L., Gu M. Preparation of Mg/Fe spinel ferrite nanoparticles from Mg/Fe-LDH microcrystallites under mild conditions. *Solid State Sciences*, 2009; Feb 28;11(2):472-478.
- Mathew D.S., Juang R.S. Structure and magnetism of spinel ferrite nanoparticles and their synthesis in microemulsions. *ChemInform*, 2007; 2;38(34).
- Oliver S.A., Willey R.J., Hamdeh H.H., Oliveri G., Busca G. Structure and magnetic properties of magnesium ferrite fine powders, *Scripta Metall Mater*, 1995; 33:1695-1701.
- Chen Q, Rondinone AJ, C. Chakoumakos B, John Zhang Z. Synthesis of superparamagnetic MgFe₂O₄ nanoparticles by coprecipitation. *J Magn Magn Mater*. 1999;194(1):1-7.
- Gusmano G., Montesperelli G., Nunziante P., Traversa E. Humidity-sensitive electrical response of sintered MgFe₂O₄, *J Mater Sci*, 1993; 28:6195-6198.
- Xiong C., Chen Q., Lu W., Gao H., Lu W., Gao Z. Novel Fe-based complex oxide catalysts for hydroxylation of phenol, *Catal Lett*, 2000; 69:231-236.
- Costa A.C., Leite A.M., Ferreira H.S., Kiminami R.H., Cava S., Gama L. Brown pigment of the nanopowder spinel ferrite

- prepared by combustion reaction. *J. Eur. Ceram. Soc.*, 2008; 31;28(10):2033-2037.
9. Alhaili M.H., Sanaullah K., Lim S., Khan A., Hipolito C.N., Abdullah M.O., Bhawani S.A, Jamil T. Photocatalytic treatment technology for palm oil mill effluent (POME) – A review, *Process Saf Environ Prot*, 2016; 102:673-686.
 10. Mohamed R.M., McKinney D.L., Sigmund W.M., Enhanced nanocatalysts, *Mater. Sci. Eng: R: Reports*, (732012) 3–7.
 11. Goldman A. *Modern Ferrite Technology*, (Springer, New York, 2006).
 12. Kinemuchi Y., Ishizaka K., Suematsu H., Jiang W., Yatsui K. Magnetic properties of nanosize NiFe_2O_4 particles synthesized by pulsed wire discharge, *Thin Solid Films*, 2002; 22;407(1):109-113.
 13. Willey R.J., Noirclerc P., Busca G. Preparation and characterization of magnesium chromite and magnesium ferrite aerogels. *Chem. Eng. Commun.*, 1993; May 1;123(1):1-6.
 14. Saffari J., Mir N., Ghanbari D., Khandan-Barani K., Hassanabadi A., Hosseini-Tabatabaei M.R. Sonochemical synthesis of $\text{Fe}_3\text{O}_4/\text{ZnO}$ magnetic nanocomposites and their application in photo-catalytic degradation of various organic dyes, *J. Mater. Sci. Mater. Electron.*, 2015;26(12):9591-9.
 15. Aliyan H., Fazaeli R., Jalilian R. $\text{Fe}_3\text{O}_4@$ mesoporous SBA-15: A magnetically recoverable catalyst for photodegradation of malachite green. *Appl. Surf. Sci.*, 2013; 276:147-53.
 16. Buthiyappan A., Aziz A., Raman A., Daud W., Ashri W.M. Recent advances and prospects of catalytic advanced oxidation process in treating textile effluents. *Rev. Chem. Eng.*, 2016; 32(1):1-47.
 17. Liu S., Sun H., Ang H.M., Tade M.O., Wang S. Integrated oxygen-doping and dye sensitization of graphitic carbon nitride for enhanced visible light photodegradation. *J. Colloid Interface Sci.*, 2016; 476:193-9.
 18. Bakre P.V., Volvoikar P.S., Vernekar A.A., Tilve S.G. Influence of acid chain length on the properties of TiO_2 prepared by sol-gel method and LC-MS studies of methylene blue photodegradation. *J. Colloid Interface Sci.*, 2016; 474:58-67.
 19. Wu X., Cai J., Li Sh., Zheng F., Lai Zh., Zhu L., Chen T., Au@ Cu_2O Stellated polytope with core-shelled nanostructure for high-performance adsorption and visible-light-driven photodegradation of cationic and anionic dyes, *J. Colloid Interface Sci.*, 2016; 479, 138-146.
 20. Mohamed Jaffer Sadiq M. and Samson Nesaraj A. Reflux condensation synthesis and characterization of Co_3O_4 nanoparticles for photocatalytic applications, *Iranian Journal of Catalysis* 4.4, 2014; pp 219-226.
 21. Teymourinia H, Salavati-Niasari M, Amiri O, Safardoust-Hojaghan H. Synthesis of graphene quantum dots from corn powder and their application in reduce charge recombination and increase free charge carriers. *J Mol Liq.* 2017;242:447-455.
 22. Hassanpour M, Safardoust-Hojaghan H, Salavati-Niasari M, Yeganeh-Faal A. Nano-sized CuO/ZnO hollow spheres: synthesis, characterization and photocatalytic performance. *J Mater Sci Mater Electron.* 2017;28(19):14678-14684.